

## Effect of the Temperature on the CO<sub>2</sub>-Corrosion of Ni<sub>3</sub>Al

J. Porcayo-Calderon<sup>1,2,\*</sup>, L.M. Martínez de la Escalera<sup>3</sup>, J. Canto<sup>3</sup>, M. Casales-Diaz<sup>2</sup>,  
V.M. Salinas-Bravo<sup>4</sup>

<sup>1</sup> Universidad Autonoma del Estado de Morelos, CIICAp, Av. Universidad 1001, 62209-Cuernavaca, Morelos, Mexico

<sup>2</sup> Universidad Nacional Autonoma de Mexico, Instituto de Ciencias Fisicas, Av. Universidad s/n, Cuernavaca, Morelos, Mexico

<sup>3</sup> Corrosion y Proteccion, Buffon 46, Mexico City, C.P. 11590, Mexico

<sup>4</sup> Instituto de Investigaciones Electricas, Av. Reforma 113, Col. Palmira, 62490-Cuernavaca, Morelos, Mexico

\*E-mail: [jporcayoc@gmail.com](mailto:jporcayoc@gmail.com)

Received: 3 December 2014 / Accepted: 19 January 2015 / Published: 24 February 2015

---

Carbon dioxide (CO<sub>2</sub>) corrosion of pipeline steels and equipment has been considered one of the most severe problems in the oil and gas industry. Carbon steels are commonly used for different purposes, because of its competitive cost. However, carbon steel is not the most corrosion resistant material for many environments. The low corrosion resistance of carbon steel is due to its inability to grow a protective oxide layer on its surface that protects it from the aggressiveness of the surrounding environment. It has been demonstrated that carbon steel can be safely operated in very corrosive service conditions if a corrosion control system is properly designed and implemented. However, when these safety precautions fail the consequences can be catastrophic. As a result, it is necessary to consider employing materials with greater corrosion resistance. In this logic intermetallic materials can be a feasible option. In this study the corrosion behavior of a Ni<sub>3</sub>Al intermetallic alloy and 1018 carbon steel was investigated. Corrosion performance of both materials was evaluated by electrochemical tests by polarization curves, rest potential measurements, and linear polarization resistance. Corrosion tests were carried out in 3% NaCl-diesel mixture saturated with CO<sub>2</sub> in a temperature gap from 30 to 80 °C. Results showed that the Ni<sub>3</sub>Al has both a nobler behavior and higher corrosion resistance than carbon steel. On the other hand, corrosion rate of carbon steel is limited by mass transfer and in case of the Ni<sub>3</sub>Al intermetallic alloy, corrosion rate is limited for its passivity.

---

**Keywords:** corrosion, carbon steel, Ni<sub>3</sub>Al, CO<sub>2</sub>, electrochemical techniques

## 1. INTRODUCTION

Metallic materials used in the petroleum and petrochemical industry are continually subjected to increasingly severe conditions. These materials require a satisfactory performance for long time regardless of higher temperatures, various flow conditions and progressively aggressive media. The sensitive part of metallic materials in these industries it is the material surface where a corrosive process is initiated. Water is the most common impurity in gas and oil and generally contains CO<sub>2</sub>. CO<sub>2</sub> is hydrated in water and carbonic acid is formed causing a process known as internal corrosion in the oil and gas industry. This kind of corrosion is defined as sweet corrosion or CO<sub>2</sub> corrosion. The formed carbonic acid is more corrosive to carbon steels than a completely dissociated acid (as HCl) having the same pH in both solutions.

Carbon steels are often used as materials in oil and gas production and transport; however, they are very susceptible to corrosion in CO<sub>2</sub> environments [1]. However, they are still widely used in oil and gas industry due to the feasible applicability and low economy. Carbon dioxide corrosion can be defined as the attack of metal by dissolved CO<sub>2</sub> in aqueous solution, and it has drawn great attention for several decades [2]. CO<sub>2</sub> corrosion on carbon steel surface is substantially an electrochemical reaction process and associated with several aqueous reaction processes, including carbon dioxide dissolution, anodic and cathodic reactions [3]. One of the inherent properties of the carbon steels is the formation of protective layers as a product of chemical and electrochemical reactions, when exposed to different environments [4, 5]. Iron carbonate (FeCO<sub>3</sub>) is one of such reaction products encountered. It modifies the kinetics of the corrosion process by forming a porous physical barrier between the electrolyte and the solid metallic surface. This barrier influences the transport of the corrosive species in the electrolyte. The protectiveness of the porous layer depends on several environmental conditions, such as iron concentration, solution pH, temperature, partial pressure of CO<sub>2</sub>, mechanical forces due to flow conditions and microstructure of the carbon steel [6]. From the economic point of view, around 55% of the damages caused by the CO<sub>2</sub> in the oil and gas industry are due to corrosion of carbon steels [7]. However, when degradation processes provoke economic losses and security risks, it is justifiable the use of more stable materials such as stainless steels and inconeles.

Intermetallic compounds are inexpensive materials with a high chemical stability. In particular nickel aluminides have been considered good candidates for applications at high temperature because of their oxidation resistance, sulfidation resistance, appropriate mechanical strength and low cost as compared to many high temperature structural materials. Nevertheless the intermetallic compounds have been developed mainly for structural applications at high temperature because of the corrosion resistance that provides them their passive layer (Al<sub>2</sub>O<sub>3</sub>) [8]. The excellent performance in these conditions has motivated their study on other work conditions like aqueous solutions. For these reasons it is of interest to understand its performance in solutions either acidic, basic, rich in chlorides, sulfur compounds, so on [9].

This work aimed to investigate the behavior in simulated oilfield solution on CO<sub>2</sub> corrosion of Ni<sub>3</sub>Al at various temperatures by electrochemical measurements. Its performance was compared against the 1018 carbon steel usually employed for construction of pipeline to transport oil.

## 2. EXPERIMENTAL PROCEDURE

### 2.1. Materials

Intermetallic alloy with nominal composition Ni-25Al (at %) was manufactured in quartz crucibles with an induction furnace in an inert atmosphere from elements of 99.99% high purity. Ingots were cooled in the furnace to room temperature and in this condition were used in the studies. For comparison purposes the performance of the 1018 carbon steel was also evaluated. The chemical composition (wt. %) of 1018 carbon steel was 0.190 C, 0.670 Mn, 0.0003 P, 0.001 S, and balance Fe. Chemical composition of the intermetallic alloy was 11.81% Al and 88.19% Ni (wt. %) determined by atomic absorption spectroscopy. The test specimens were cut into squares of 5.0 x 5.0 x 3.0 mm using a diamond tipped blade. For electrical connection, specimens were spot-welded to a Ni20Cr wire, and then mounted in thermosetting resin. Sample surfaces were ground to 600 grade emery paper then first rinsed with distilled water and later by ethanol in an ultrasonic bath for 10 minutes. Specimens with this surface condition were employed as the working electrode (WE) in the electrochemical tests.

### 2.2. Electrochemical measurements

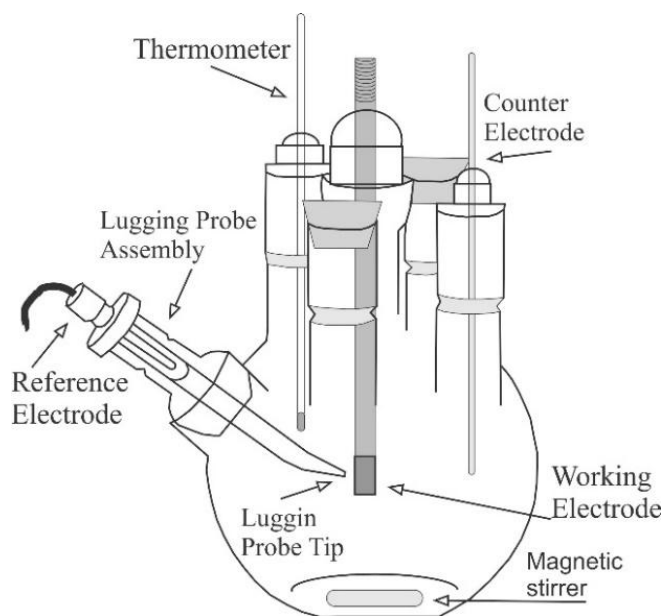


**Figure 1.** Scheme showing the experimental set-up for electrochemical measurements.

Testing solution consisted of 3% NaCl + 10% diesel emulsion, heated, de-aerated by purging with CO<sub>2</sub> gas during 2 hours prior the experiment and kept bubbling throughout the experiment. The electrochemical cell used was that described by standard ASTM G5 and shown on figure 1. Test temperatures were 30, 40, 50, 60, 70 and 80 °C. Electrochemical tests were carried out using an ACM Instruments zero-resistance ammeter (ZRA) coupled to a personal computer. A typical three electrodes arrangement was used, the reference electrode (RE) was a saturated calomel electrode (SCE, 0.242V vs. SHE) and the counter electrode (CE) was a platinum wire. All the potentials described in the text

are relative to the SCE, unless stated differently. For each electrochemical test a volume of 600 ml of fresh solution was used. Polarization curves were recorded at a constant sweep rate of 1 mV/s, and the scanning range was from  $-400$  to  $+700$  mV versus the open circuit potential,  $E_{corr}$  (ASTM G5-04 and ASTM G-3-04). To assess the capability of the different materials to form a protective oxide scale on their surfaces upon immersion in the testing solution the free corrosion potential as a function of time of the working electrodes  $E_{corr}$ , was measured versus a SCE for 50 hours. Linear polarization curves were obtained by polarizing the specimens from  $-30$  to  $30$  mV versus the free corrosion potential value,  $E_{corr}$ , at a scanning rate of 1 mV/s, measurements were made for 50 hours. After testing, corroded specimens were analyzed in a DSM 960 Carl Zeiss scanning electronic microscope (SEM).

### 3. RESULTS AND DISCUSSION

#### 3.1. Microstructural analysis

Figure 2 shows the microstructure of the  $Ni_3Al$  intermetallic. During solidification of an alloy with stoichiometry close to that of  $Ni_3Al$ , in the liquid phase there is a competition from phase stability between  $\beta$  (NiAl),  $\gamma'$  ( $Ni_3Al$ ),  $\gamma$  (Ni) with stable eutectic phases ( $\beta$ - $\gamma'$ ), metastable ( $\beta$ - $\gamma$ ) and peritectic ( $\gamma'$ - $\gamma$ ) which have common borders in the Ni-Al binary diagram. Because the region of phase stability  $\gamma'$  is very narrow and any deviation in the Ni/Al ratio favor the stability of any of the aforementioned phases, ie, an increase in Ni content tends to favor the stability of  $\gamma'$ - $\gamma$  phase. According to Verin [10] the microstructure of the Ni-23Al-0.001Ce-0.004Co (at %) is a combination of dendritic  $\gamma'$  and  $\gamma$  phases where the matrix is the  $\gamma'$  and the interdendritic is the  $\gamma$  phase, similar results were obtained by Chiba and Hanada [11] for alloys Ni-23Al (at%) and Jozwik et al [12] for the alloy Ni-22Al-0.002Zr-0.001B (at %).

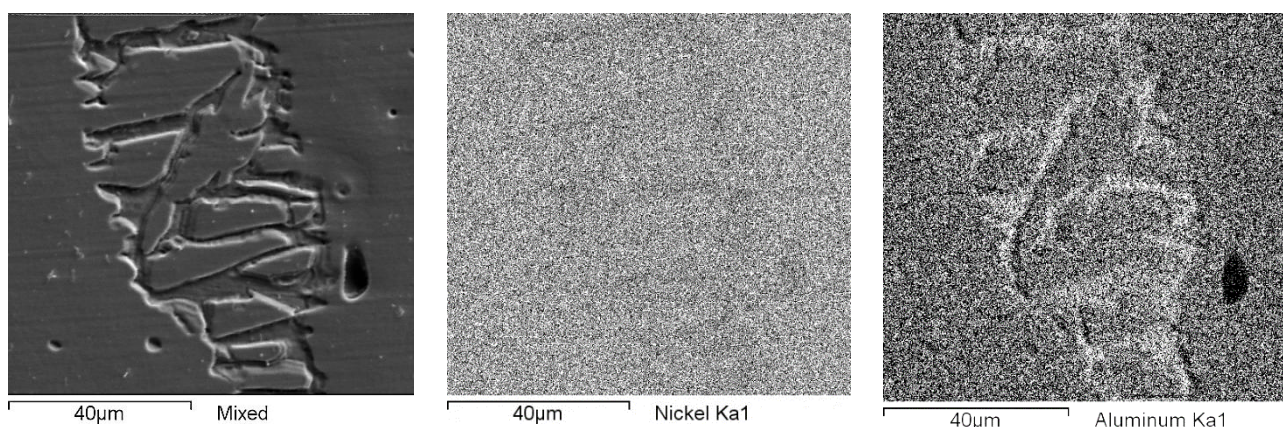


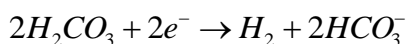
**Figure 2.** Microstructure of intermetallic alloy  $Ni_3Al$ .

Moreover Hunziker and Kurz [13] mentioned that the directional solidification of intermetallic Ni-25Al (at%) shows a microstructure where  $\beta$ ,  $\gamma$  and  $\gamma'$  phases are found, in this case,  $\gamma'$  phase is

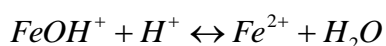
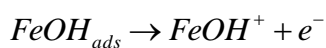
originated during cooling of metastable eutectic  $\beta$ - $\gamma$ . It has been shown that there are subsequent transformations after solidification process, which complicates the interpretation of generated phases. According to the observed microstructure of the intermetallic alloy tested, it consists of two phases where the matrix corresponds to  $\gamma$ - $\gamma'$  and a  $\beta$ - $\gamma'$  dendritic phase as indicated by Hunziker and Kurz [14] and Rosas et al [15]. This type of microstructure is characteristic of the  $\text{Ni}_3\text{Al}$  intermetallic and its formation is attributed to the difference between the melting points of the constituent phases. According to Lee et al [16, 17], in liquid phase,  $\gamma$  is the more stable phase and during the solidification process,  $\gamma$  solidifies first and favors the formation of dendritic structures composed of phases that are still in liquid state ( $\beta$ - $\gamma'$ ). During the cooling process  $\gamma$  fraction decreases while  $\gamma'$  increases. No precipitates were observed in the interdendritic region of the alloys.

### 3.2. Polarization curves

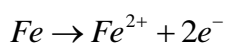
The potentiodynamic polarization curves for the corrosion of carbon steel and  $\text{Ni}_3\text{Al}$  in solution of 3% NaCl-diesel (90:10 ratio) with  $\text{CO}_2$  at different temperatures are shown in figure 3 and 4, respectively. Potentiodynamic polarization measurement of metals and alloys indicates the tendency of a metal to undergo active, passive and transpassive behaviors [18]. Figure 3 shows that the cathodic branch has the same shape and tendency at all temperatures. This indicates that the reduction reaction is the same, and it is thermally activated because both its slope increases and there is a shift of the cathodic branch to larger current densities as temperature increases. According to the chemical composition of the test solution employed, the cathodic reaction corresponds to the reduction of the carbonic acid [19, 20]:



Cathodic curves show a trend known as non-Tafel slope, where this is a characteristic of a processes controlled by mass transfer [21, 22]. According to the trend of the anodic branch, the carbon steel is undergone a continuous dissolution process throughout the range of potential evaluated. Nevertheless, it has been suggested that the dissolution of Fe is the result of a sequential mechanism that involves the presence of intermediates [23, 24]:



The anodic dissolution reaction can be summarized as [19, 20]:



In all cases it is observed that the corrosion potential,  $E_{corr}$ , is around -730 to -760 mV, with a shift toward more positive potentials by increasing the temperature. The increase in corrosion rate by increasing temperature is attributed to mass transfer of the reactive ion. [23]. The potentiodynamic polarization parameters containing corrosion potential, corrosion current density and Tafel slopes are listed in table I. In table I two  $I_{corr}$  values are shown. They were calculated from both anodic and cathodic branches. It is reported that in the case of this type of corrosive systems (saturated with  $CO_2$ ) the corrosion reactions are limited by mass transfer (carbonic acid), and it is suggested that the  $I_{corr}$  value should be determined from the cathodic branch [21, 22].

**Table I.** Electrochemical parameters for carbon steel tested in 3% NaCl-diesel saturated with  $CO_2$  at different temperatures.

Temperature (°C)	Material	$E_{corr}$ (mV)	$b_a$ (mV/Dec)	$b_c$ (mV/Dec)	Anodic $I_{corr}$ (mA/cm <sup>2</sup> )	Cathodic $I_{corr}$ (mA/cm <sup>2</sup> )
30	1018	-727	73	208	0.218801	0.04257
40	1018	-745	76	199	0.2534065	0.0595
50	1018	-743	81	219	0.37761	0.11785
60	1018	-731	101	269	0.435357	0.151344
70	1018	-733	81	265	0.46018	0.189672
80	1018	-727	76	240	0.573437	0.21859

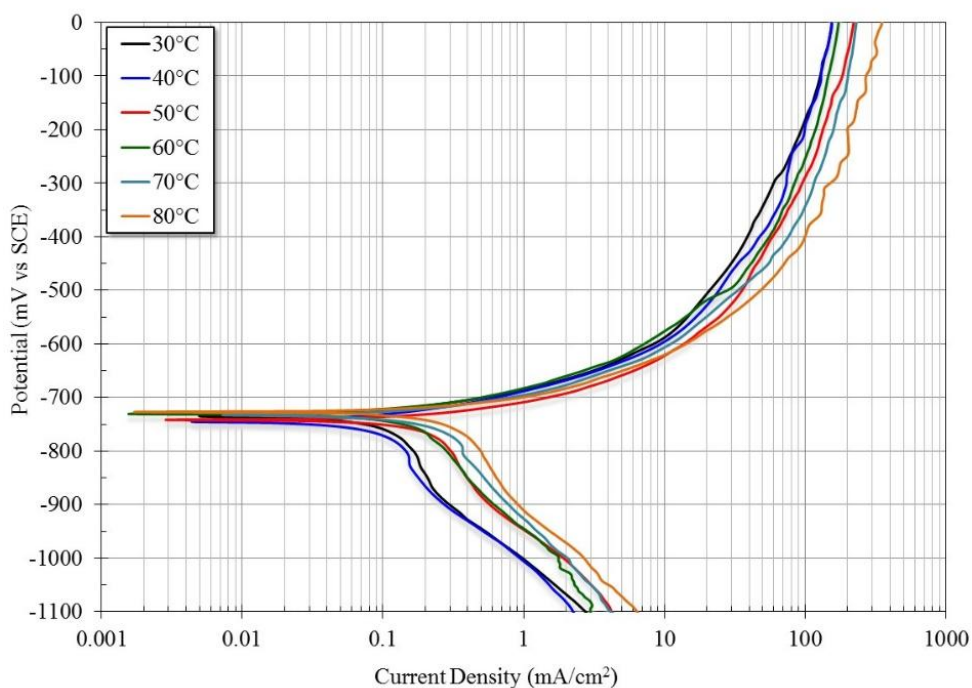


**Figure 3.** Potentiodynamic polarization for carbon steel in 3% NaCl + diesel with  $CO_2$  at different temperatures.

It has been reported that the presence of NaCl and carboxylic acids decreases anodic Tafel slopes (*ba*) and increases cathodic Tafel slopes. Moreover, *I<sub>corr</sub>* values increase 3-4 times with increasing temperature [25]. On the other hand, research conducted by Zhang et. al [23] on API X65 steel in 5% NaCl solution saturated with CO<sub>2</sub> from 25 to 75 °C, show similar results to those reported in Table I. The differences in their results with those reported here may be due mainly to the presence of the oil phase. According to other studies water-soluble fractions (WSF's) affects the mass transfer process, and provides protection for carbon steel, increasing its resistance to corrosion [26].

*I<sub>corr</sub>* values calculated from the anodic branch are much larger than those obtained from the cathodic branch. *I<sub>corr</sub>* values calculated from Tafel curves of both branches must be the same, however when there are mass transfer limitations, limiting currents are observed in the cathodic branch and this indicates that the limiting reaction of the corrosion process is the transport of species to the electrode surface.

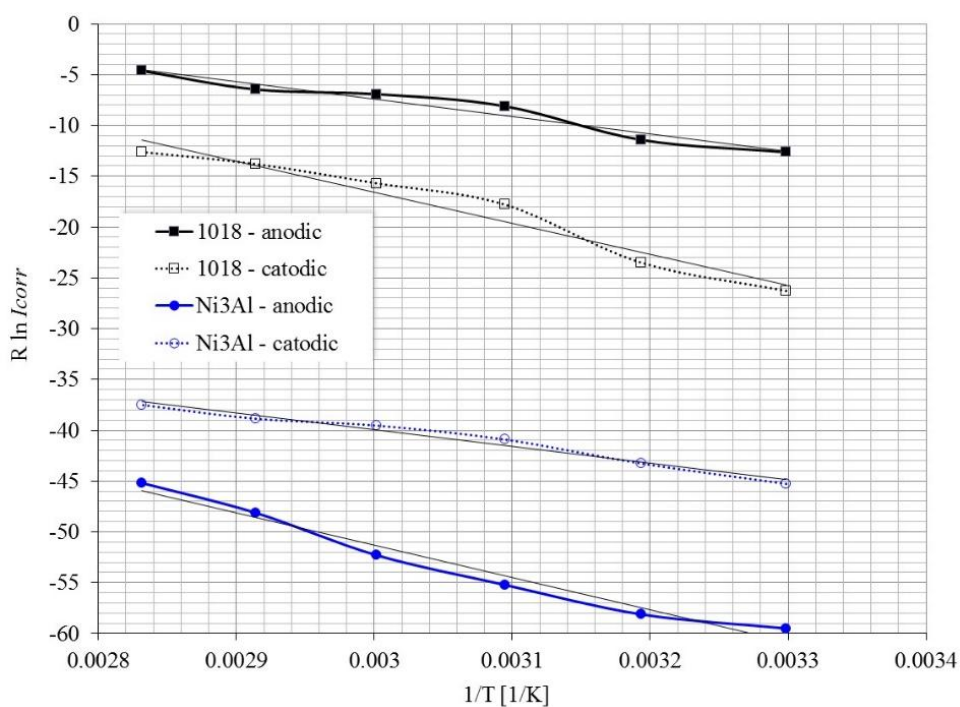


**Figure 4.** *R ln (I<sub>corr</sub>) - 1/T* relationship for 1018 carbon steel and Ni<sub>3</sub>Al in diesel-brine saturated with CO<sub>2</sub>.

The dependence of the rate of a metal dissolution process on temperature can be explained by using an Arrhenius type equation, where the activation energy of the cathodic and anodic reactions can be calculated according to [23]:

$$I_{corr} = k \exp\left(-\frac{\Delta E}{RT}\right)$$

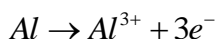
Rearranging:

$$R \ln(I_{corr}) = R \ln k - \frac{1}{T} \Delta E$$

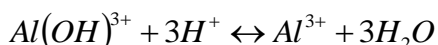
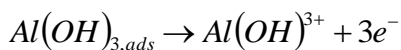
Where  $\Delta E$  ( $\text{J mol}^{-1}$ ) is the activation energy which can be obtained from the slope of the relation  $R \ln(I_{corr})$  vs  $1/T$ .  $k$  is a constant and  $R$  is the gas constant ( $8.314472 \text{ J/K-mol}$ ). In figure 4 the relation  $R \ln(I_{corr}) - 1/T$  is shown. From the slope of the lines shown in figure 4, the activation energy of the anodic and cathodic reaction was obtained. The results were  $17.25$  and  $30.54 \text{ kJ mol}^{-1}$  respectively. This implies that the oxidation reaction (anodic reaction) of carbon steel is faster than the reduction reaction (cathodic reaction) of carbonic acid, and therefore the rate limiting step of the overall corrosion process is the latter.

Zhang et. al [23] reported activation energies of  $14.39 \text{ kJ mol}^{-1}$  for API X65 steel in 5% NaCl solution saturated with  $\text{CO}_2$ , this value is quite low compared to  $30.54 \text{ kJ mol}^{-1}$  reported here. The main difference in the experimental conditions of Zhang et. al is the absence of diesel. This implies that the presence of diesel and particularly a WSF's contribute to this increase in the activation energy which brings on an increase in the corrosion resistance of 1018 carbon steel.

In Figure 5 shows potentiodynamic polarization curves for the  $\text{Ni}_3\text{Al}$  in 3% NaCl-diesel mixture saturated with  $\text{CO}_2$  at different temperatures. It is observed that the cathodic branches have the same shape and tendency at all temperatures evaluated. This is because the reduction reaction is the same, and is thermally activated. The slope shows a tendency to increase and in addition there is a shift to higher current densities by increasing the temperature. The corrosion potential,  $E_{corr}$ , span from  $-420$  to  $-440$  with a shift to more positive potential by increasing temperature. This displacement is less than that observed in the carbon steel, and  $E_{corr}$  values also are more positive than those obtained with carbon steel. This indicates that the  $\text{Ni}_3\text{Al}$  intermetallic compound has a nobler behavior than the carbon steel. Moreover, the anodic branch exhibits a dissolution process less active than that observed with carbon steel (smaller increase in current density by increasing the potential or increased slope of the anodic branch). At  $30$  and  $40 \text{ }^\circ\text{C}$ , there is a passive region between  $-250$  and  $-100 \text{ mV}$ . At higher temperatures above  $E_{corr}$ , there is a more active dissolution process, and at a potential of about  $-100 \text{ mV}$  an attempt to grow a passive zone is observed. The breakdown of passive oxide films by aggressive anions such as halides on alloys containing Al at sufficiently positive anodic potentials is frequently responsible for the failure of these alloys in aqueous halide solutions and as it usually results in severe pitting of the underlying metal [27]. It is known that the protective oxide on the Ni-Al intermetallic is  $\text{Al}_2\text{O}_3$ , so it is possible that the anode reaction is:



This reaction is the result of a sequential reaction mechanism with intermediates according to



The potentiodynamic polarization results of Ni<sub>3</sub>Al are listed in table II. Likewise two *I<sub>corr</sub>* values are reported. They were calculated from both the anodic and cathodic branch. It is noticed that the *I<sub>corr</sub>* values calculated from the anodic branch are smaller than those obtained from the cathodic branch. This indicates that the limiting step of the corrosion process is the corrosion resistance of the intermetallic compound, and not the transport of species at the working electrode surface.

**Table II.** Electrochemical results for Ni<sub>3</sub>Al tested in 3% NaCl-diesel mixture saturated with CO<sub>2</sub> at different temperatures.

Temperature (°C)	Material	<i>E<sub>corr</sub></i> (mV)	<i>b<sub>a</sub></i> (mV/Dec)	<i>b<sub>c</sub></i> (mV/Dec)	Anodic <i>I<sub>corr</sub></i> (mA/cm <sup>2</sup> )	Cathodic <i>I<sub>corr</sub></i> (mA/cm <sup>2</sup> )
30	Ni <sub>3</sub> Al	-432	99	180	0.00078	0.004321
40	Ni <sub>3</sub> Al	-433	55	202	0.00092137	0.00551
50	Ni <sub>3</sub> Al	-434	80	215	0.001307	0.00731
60	Ni <sub>3</sub> Al	-436	101	238	0.0018552	0.0086197
70	Ni <sub>3</sub> Al	-438	82	205	0.0030616	0.009346
80	Ni <sub>3</sub> Al	-440	88	206	0.00436	0.011

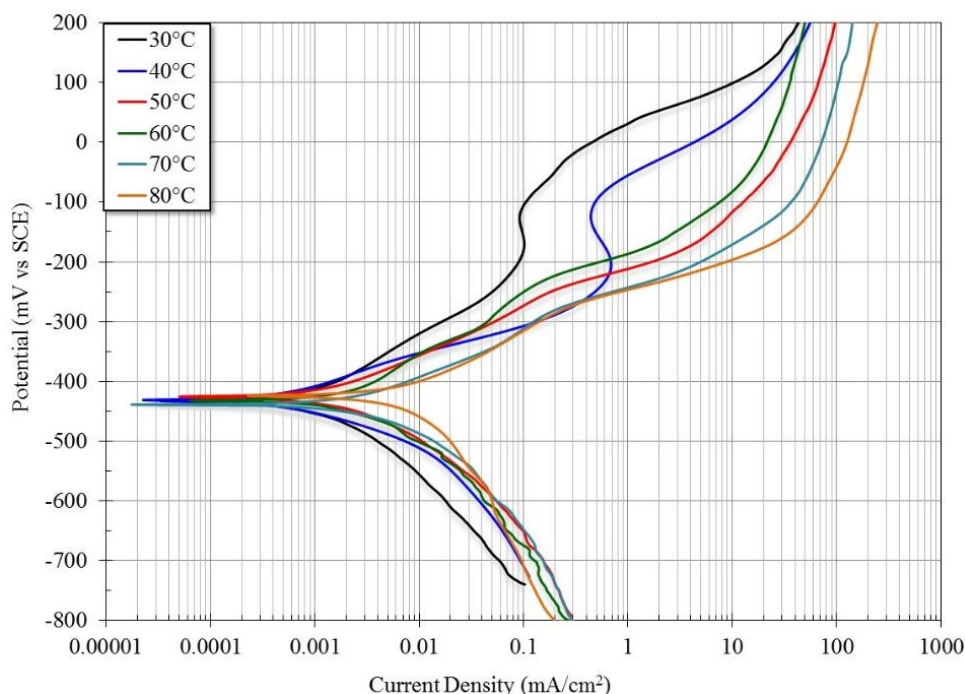


**Figure 5.** Potentiodynamic polarization for Ni<sub>3</sub>Al in 3% NaCl + diesel with CO<sub>2</sub> at different temperatures.

Figure 6 shows *I<sub>corr</sub>* values obtained from extrapolation of the anodic and cathodic curves as a function of temperature for both materials. From this figure it can be seen that the intermetallic

compound has a higher resistance to corrosion than 1018 carbon steel at all temperatures, and that these differences are up to two orders of magnitude. This highlights the corrosion resistance of the intermetallic compound. Similarly, Figure 4 shows that the activation energy of the anodic and cathodic reaction rates are 31.74 and 16.44 kJ mol<sup>-1</sup>, respectively. This indicates that the reduction reaction (cathodic reaction) of carbonic acid is faster than the oxidation reaction (anodic reaction) of Ni<sub>3</sub>Al, and therefore the rate limiting step of the overall corrosion process is the material passivity. Also it is well known that temperature has a profound influence on the coefficients and diffusion rates, which are also explained by an Arrhenius type equation. Therefore, the smallest value of the activation energy for 1018 carbon steel implies a highest value of diffusion coefficients in the solution [28].

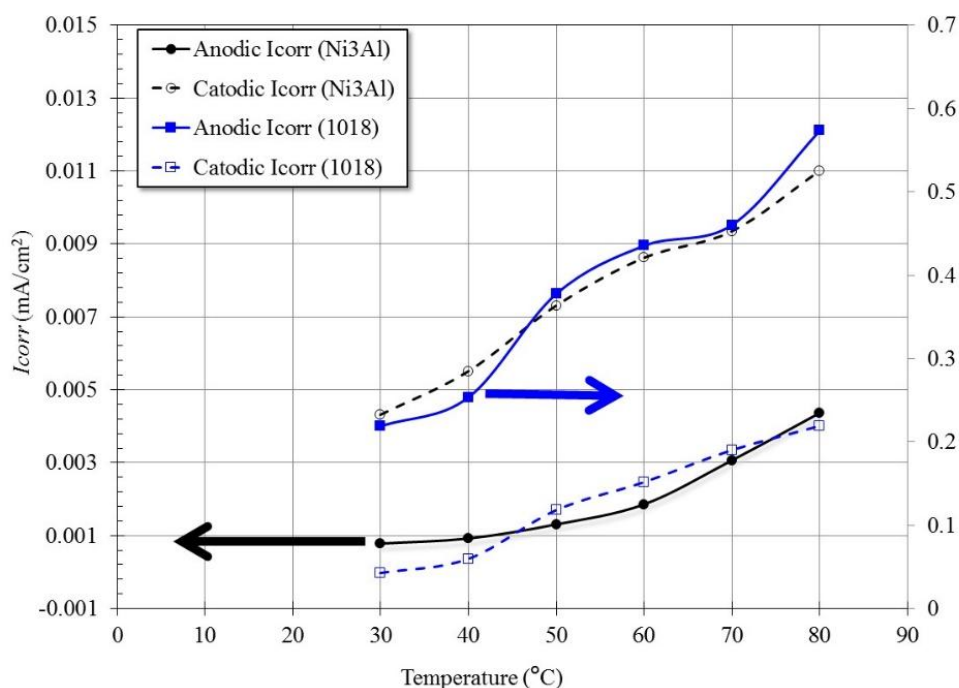


**Figure 6.** *I<sub>corr</sub>* values obtained from the anodic and cathodic curves for 1018 carbon steel and intermetallic compound Ni<sub>3</sub>Al.

### 3.3. Free Corrosion Potential Curves

The free corrosion potential experiments of carbon steel and Ni<sub>3</sub>Al in a mixture of 3% NaCl-diesel (90:10 ratio) with CO<sub>2</sub> at different temperatures are shown in figure 7 and 8, respectively. *E<sub>corr</sub>* gives a relative thermodynamic rating of a metal or alloy in a given environment. Usually a rise of potential in the positive direction indicates the formation of a passive film, and a steady potential indicates that the film remains intact and protective. A drop of potential in the negative direction indicates breaks in the film, dissolution of the film, or no film formation [29]. Figure 7 shows that the corrosion potentials (*E<sub>corr</sub>*) shift towards a positive direction as time elapses. It is important to note that in the 50 hours of test corrosion potential fluctuated between 15 and 20 mV at all temperatures. This tendency is due to the formation of a protective layer on the carbon steel surface.

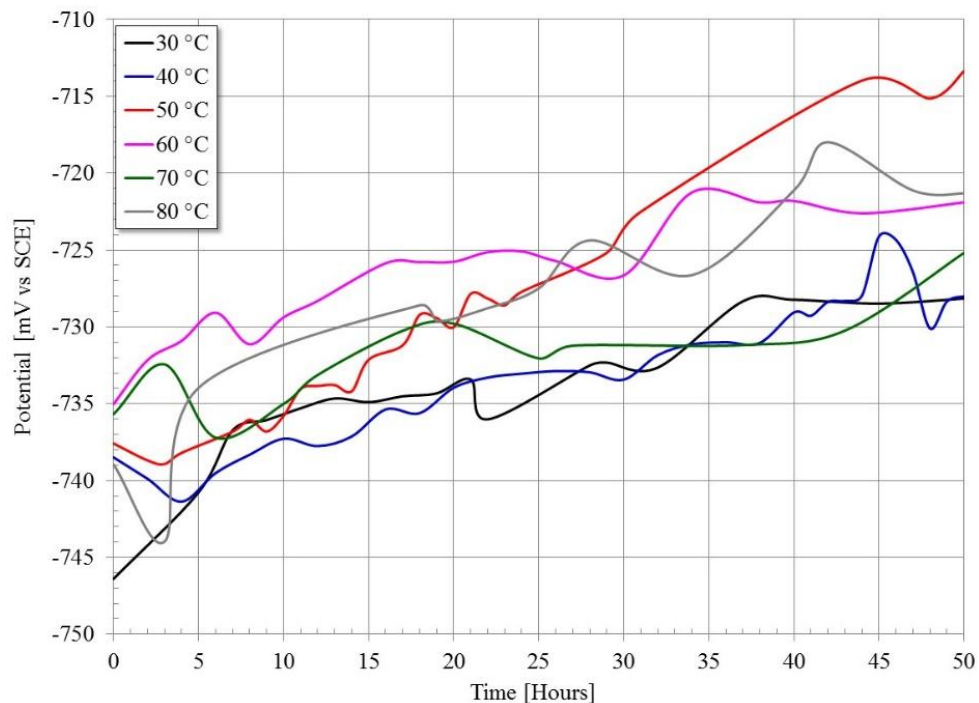


**Figure 7.** Change of the *E<sub>corr</sub>* values as function of testing time for carbon steel in 3% NaCl + diesel with CO<sub>2</sub> at different temperatures.

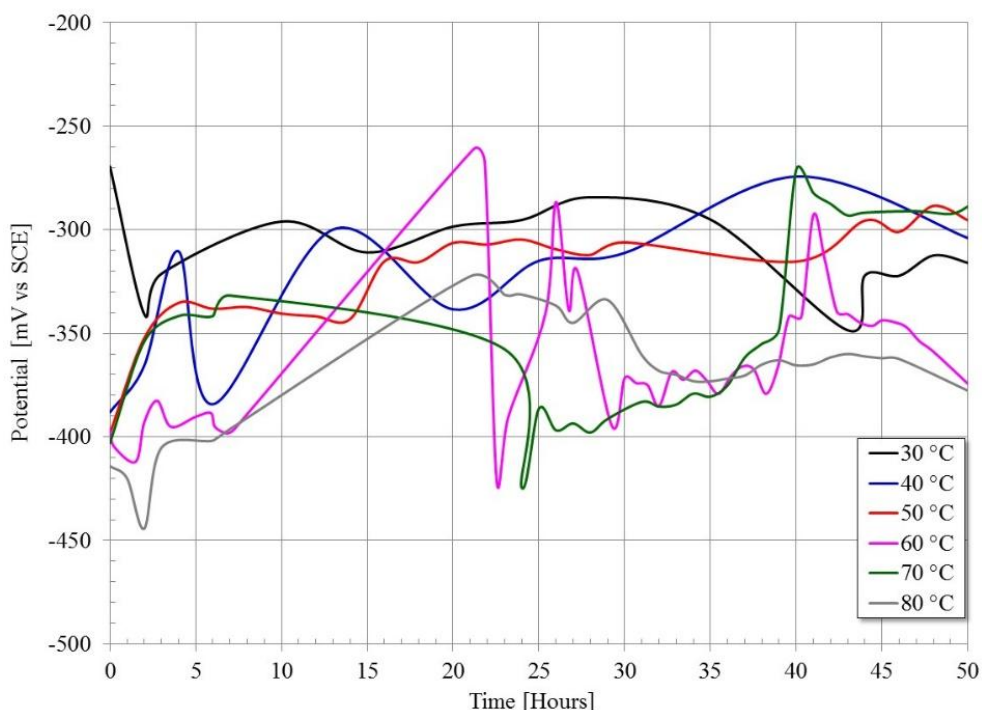


**Figure 8.** Change of the *E<sub>corr</sub>* values as function of testing time for Ni<sub>3</sub>Al in 3% NaCl + diesel with CO<sub>2</sub> at different temperatures.

However, slight fluctuations are observed indicating the breakdown of the passive layer or the formation of pitting. At 30 and 40 °C, the rate of change (slope of the curves) is similar, and the

maximum is observed at 50 °C. At higher temperatures there is no consistent trend. This indicates that the formation of the passive layer is more favorable at 50 °C for the experimental conditions reported here. Figure 8 shows that for the Ni<sub>3</sub>Al, corrosion potentials showed an extensive change. The fluctuations are greater at temperatures above 50 °C. The abrupt fluctuations in  $E_{corr}$  values may be due to the susceptibility of pitting corrosion, but it is evident that there is an immediate tendency to self-healing of its passive layer. Ability of alloys to passivate during a long period of time depend on rates of several processes such as formation of oxide at the metal/oxide interface, ionic transport across oxide and dissolution of oxide at the oxide/electrolyte interface [30].

### 3.4. Linear Polarization Curves

Change of  $I_{corr}$  obtained by linear polarization measurements is given in figures 9 and 10. It is known that once polarization resistance is determined, calculation of  $I_{corr}$  requires knowledge of the Tafel constants, and these constants can be determined from experimental polarization curves. Values of  $I_{corr}$  were obtained from the polarization resistance measurements using Stern-Geary equation [31].

$$i_{corr} = \frac{b_a b_c}{2.303 R_p (b_a + b_c)}$$

where  $b_a$  and  $b_c$  values were those reported in Table I and II.

Figure 9 shows an increase in  $I_{corr}$  values as time elapses. The increases are greater at 60 and 70 °C. Corrosion rate observed at 80 °C is comparable to that observed at 30 °C. Only at 50 °C a decrease in the initial values of  $I_{corr}$  was observed and then fluctuates around 0.3 mA/cm<sup>2</sup>. It has been reported that the temperature affects the corrosion rate in two ways. First, in case that a protective layer is not formed on the steel surface, temperature rising leads to an increase in corrosion rate. Second, when there is a suitable condition for iron carbonate precipitation, in this case a temperature rise increases the precipitation rate. Therefore, in equal time base, the protective layer forms more quickly at higher temperatures than at lower ones. Hence, the corrosion rate at higher temperatures becomes lower because a good protective layer forms on the steel surface [32]. The reason why at 60 and 70 °C higher corrosion rates have been obtained is uncertain since it has been observed that the formation of a protective corrosion product films in CO<sub>2</sub> is complex and is influenced by environmental conditions, such as iron concentration, solution pH, temperature, partial pressure of CO<sub>2</sub>, mechanical forces present in the flow and microstructure of the carbon steel. However, CO<sub>2</sub> supersaturation level is a crucial factor, and has an indirect effect during the entire corrosion progress. On the other hand, the FeCO<sub>3</sub> supersaturation in the solution has an important effect on the growth and nucleation of FeCO<sub>3</sub> crystal. The formation of iron carbonate on steel surface is one of the important factors influencing the rate of corrosion [33-36]. Gao et al [37] state that at the beginning of CO<sub>2</sub> corrosion the corrosion rate could be high because of the presence of cementite (Fe<sub>3</sub>C) and ferrite (α-Fe). Where ferrite is dissolved due to its higher energy and electric potential and the cementite can be the cathodic site because

cementite is a metallic conductor with low hydrogen overvoltage and this galvanic coupling encourage the possibility of  $\text{FeCO}_3$  precipitation around cementite. However, the  $\text{FeCO}_3$  films would be porous and loose if the nucleation rate is low, regardless of the crystal growth. If the porosity of the  $\text{FeCO}_3$  films is so large that allows solution to permeate, then the protection level provided is not sufficient to prevent corrosion. Corrosion product films with low porosity protect more effectively the steel surface from permeation of the solution [37].

Figure 10 show the change of  $I_{\text{corr}}$  values of the  $\text{Ni}_3\text{Al}$  intermetallic. In general,  $I_{\text{corr}}$  values are smaller than those of carbon steel (up to two orders of magnitude). In the first 5 hours of immersion a decrease in the  $I_{\text{corr}}$  values is observed, but after that, large fluctuations are observed. At 50 °C, a stable behavior is observed in  $I_{\text{corr}}$  values, but with a tendency to increase. At 80 °C, after 20 hours of testing more stable values were obtained. Fluctuations in  $I_{\text{corr}}$  values indicate the dissolution of the passive layer or the presence of localized attack. It is well known that the  $\text{Al}_2\text{O}_3$ -forming alloys exhibit a passive behavior in aqueous solutions due to the thin compact oxide film on its surface. Chemical composition, pH and temperature influence the corrosion behavior by changing the solubility of the oxide film. In neutral NaCl solutions the protective film has low solubility although chloride ion is known to increase solution corrosiveness. Further, when  $\text{CO}_2$  is in solution the formation of  $\text{H}^+$  and  $\text{CO}_3^{2-}$  will enhance the conductivity and acidity of the electrolyte rather quickly, and the pH solution can be lowered up to 4.0 [38]. Also it has been reported that the addition of carboxylic acid (similar to the carbonic acid) enhances the solubility of the oxide layer, which led to higher corrosion rates. In this case the chloride ions act as partners in the electrochemical reaction. [25]

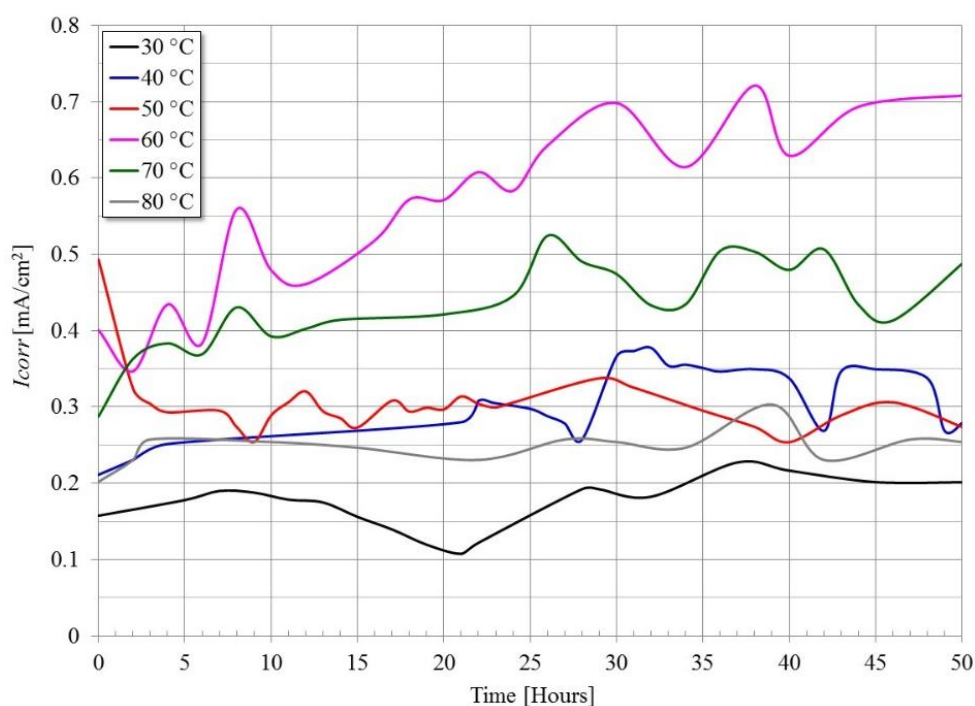


**Figure 9.** Change of  $I_{\text{corr}}$  with time for carbon steel in 3% NaCl + diesel with  $\text{CO}_2$  at different temperatures.

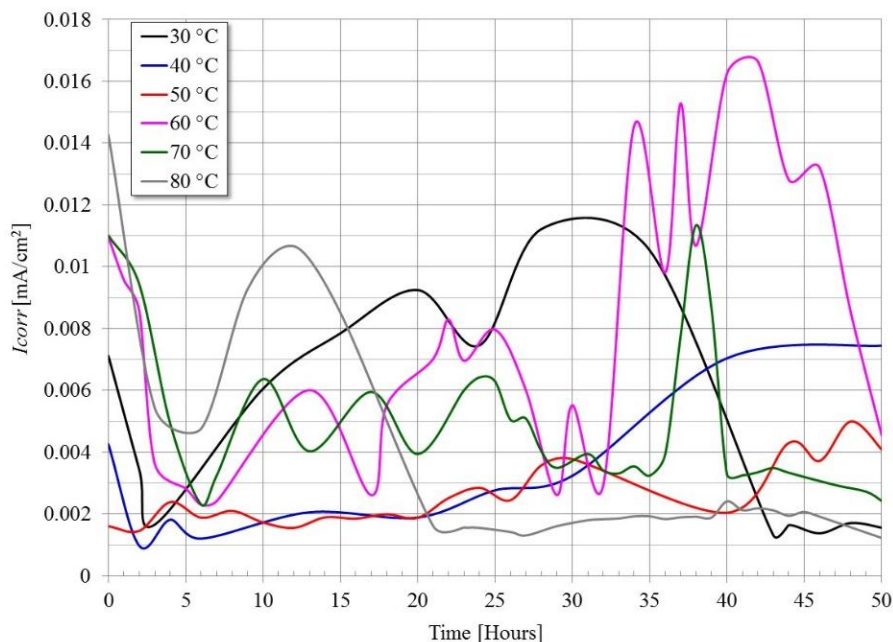
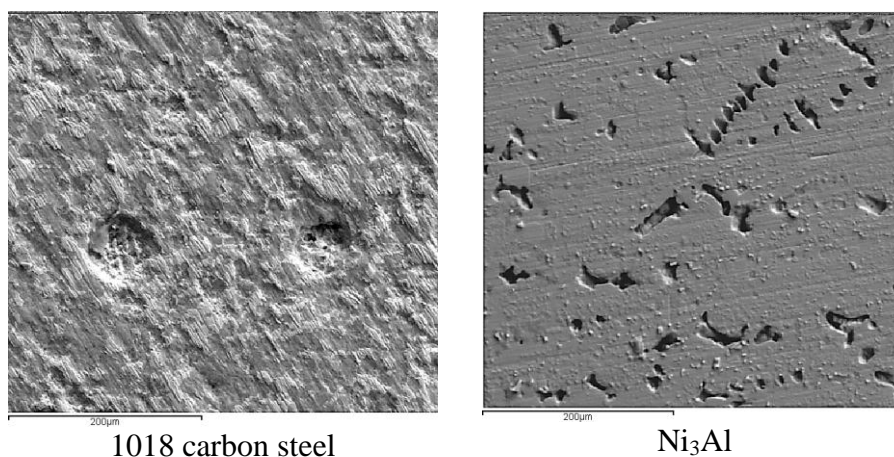


**Figure 10.** Change of  $I_{corr}$  with time for  $Ni_3Al$  in 3% NaCl + diesel with  $CO_2$  at different temperatures.

Figure 11 shows the superficial aspects of the test electrodes used as working electrodes in the electrochemical tests evaluated at 40 °C. Superficial aspects at other temperatures were similar to those shown here. The superficial attack undergone by the carbon steel corresponds to that defined as generalized corrosion with localized attack (pitting). On the other hand, the intermetallic showed only localized attack (dissolution) in dendritic phases. This localized attack is the reason for the large fluctuations observed in measurements of  $I_{corr}$ . Once the dendritic phases were dissolved  $I_{corr}$  values remain stable (Figure 10). The matrix phase of the intermetallic alloy did not show a significant attack it only showed the presence of lines generated by the grinding process. Similar aspects have been observed for aluminum alloys in NaCl solutions in presence of carboxylic acids [25].



1018 carbon steel

$Ni_3Al$

**Figure 11.** Superficial aspect of tested electrodes at 40 °C.

#### 4. CONCLUSIONS

A study on the corrosion performance of Ni<sub>3</sub>Al intermetallic alloy in brine-diesel saturated with CO<sub>2</sub> from 30 to 80°C has been carried out using electrochemical techniques. For comparison, the same tests were performed with commercial 1018 carbon steel. Results clearly show that the intermetallic compound Ni<sub>3</sub>Al has a high corrosion resistance at all temperatures tested. Corrosion of carbon steel is controlled by mass transfer of carbonic acid (cathodic reaction) to the surface of the working electrode, and the superficial attack experienced corresponds to that defined as generalized corrosion with pitting attack. Furthermore, the rate of corrosion of the intermetallic Ni<sub>3</sub>Al is at least two orders of magnitude less than that of carbon steel and the corrosion rate is controlled by the rate of dissolution (anodic reaction) of the dendritic phase causing localized corrosion.

#### ACKNOWLEDGEMENTS

Financial support from Consejo Nacional de Ciencia y Tecnología (CONACYT, México) (Project 198687) is gratefully acknowledged. The authors acknowledge the support of D. Lopez-Dominguez (Instituto Tecnológico de Zacatepec) during his Professional Residence at the Instituto de Ciencias Físicas-UNAM.

#### Conflict of Interests

The authors declare that there is no conflict of interests regarding the publication of this paper.

#### References

1. G. Schmitt, *Corrosion/83*, NACE, Paper No. 43. (1983).
2. C. De Waard and D.E. Williams, *Corrosion*, 31 (1975) 177-82.
3. E. Dayalan, F.D. de Moraes, J.R. Shadley, E.F. Rybicki, and S.A. Shirazi, *Corrosion/98*, NACE, Paper No. 51 (1998).
4. A. Pfenning, R. Bäbler, *Corrosion Science*, 51 (2009) 931-940.
5. K. Gao, F. Yu, X. Pang, G. Zhang, L. Qiao, W. Chu, M. Lu, *Corrosion Science*, 50 (2008) 2796-2803.
6. F. Farelas, M. Galicia, B. Brown, S. Nesic, H. Castaneda, *Corrosion Science*, 52 (2010) 509–517.
7. S. Nešić, *Corrosion Science*, 49 (2007) 4308–4338.
8. P.F. Tortorelli, K. Natesan, *Materials Science and Engineering: A*, 258 (1998) 115-125.
9. M.C. García-Alonso, M.F. López, M.L. Escudero, J.L. González-Carrasco, D.G. Morris, *Intermetallics*, 7 (1999) 185–191.
10. A.S. Verin, *Metal Science and Heat Treatment*, 36 (1994) 99-102.
11. A. Chiba, S. Hanada, *Intermetallics*, 4, (1996) 55-59.
12. P. Jozwik, E. Jezierska, Z. Bojar, *Materials Chemistry and Physics*, 81 (2003) 448-451.
13. O. Hunziker, W. Kurz, *Acta Materialia*, 45 (1997) 4981-4992.
14. O. Hunziker, W. Kurz, *Metallurgical and Materials Transactions A: Physical Metallurgy and Materials Science*, 30 (1999) 3167-3175.
15. G. Rosas, R. Esparza, A. Bedolla, O. Flores, R. Perez, *Adv. in Tech. of Mat. and Mat. Proc.*, 9 (2007) 99-102.
16. D. Lee, M.L. Santella, I.M. Anderson, G.M. Pharr, *Intermetallics*, 13 (2005) 187-196.

17. D.B. Lee, M.L. Santella, *Materials Science and Engineering A*, 374 (2004) 217-223.
18. B.G. Ateya, F.M. Al Kharafi, R.M. Abdalla, *Materials Chemistry and Physics*, 78 (2002) 534-541.
19. D.A. López; T. Pérez, S.N. Simison, *Materials and Design*, 24 (2003) 561-575.
20. H.M. Ezuber, *Materials and Design*, 30 (2009) 3420-3427.
21. X. Liu, P.C. Okafor, Y.G. Zheng, *Corrosion Science*, 51 (2009) 744-751.
22. L.M. Rivera-Grau, M. Casales, I. Regla, D.M. Ortega-Toledo, J.A. Ascencio-Gutierrez, J. Porcayo-Calderon, L. Martinez-Gomez, *International Journal of Electrochemical Science*, 2013 (2013) 2491-2503.
23. G. Zhang, Ch. Chen, M. Lu, Ch. Chai, Y. Wu, *Materials Chemistry and Physics*, 105 (2007) 331-340.
24. J.O'M. Bockris, D. Drazic, *Electrochimical Acta*, 7(1962) 293-313.
25. A. Al Mayouf, L. Al Fuhaiman and A. Suhaybani, *Anti-Corrosion Methods and Materials*, 55 (2008) 79-85.
26. J. Porcayo-Calderon, M. Casales, L.M. Rivera-Grau, D.M. Ortega-Toledo, J.A. Ascencio-Gutierrez, L. Martinez-Gomez, *Journal of Chemistry*, 2014, Volume 2014, Article ID 940579, 10 pages, <http://dx.doi.org/10.1155/2014/940579>.
27. M.G. Mahjani, M. Sabzali, M. Fafarian, *Anti-Corrosion Methods and Materials*, 55 (2008) 208-216.
28. Hong-Joo Lee, Duk-Won Kang and Young Ju Lee, *Korean J. Chem. Eng.*, 21 (2004) 895-900.
29. I. Gurappa, *Materials Characterization*, 49 (2002) 73-79.
30. M.C.R.A. Rezende, A.P.R. Alves, E.N. Codaro and C.A.M. Dutra, *Mater. Science: Materials in Medicine*, 18 (2007) 149-154.
31. E.E. Stansbury and R.A. Buchanan, *Fundamentals of Electrochemical Corrosion*, ASM International, Ohio (2000).
32. M. Shayegani, M. Ghorbani, A. Afshar and M. Rahmaniyan, *Corrosion Engineering, Science and Technology*, 44 (2009) 128-136.
33. A. Dugstad, *CORROSION/92*, Houston, TX, USA, 1992, NACE International, paper no. 14.
34. J.L. Crolet, N. Thevenot, S. Nešic, *CORROSION/96*, paper no. 4 (Houston, TX: NACE, 1996).
35. E.W.J. van Hunnik, B.F.M. Pots, E.L.J.A. Hendriksen, *CORROSION/96*, paper no. 6, (Houston, TX: NACE International, 1996).
36. A. Dugstad, *CORROSION/98*, paper no. 31, (Houston, TX: NACE International, 1998).
37. M. Gao, X. Pang, K. Gao, *Corrosion Science*, 53 (2011) 557-568.
38. Qing Qu, Jie Ma, Lin Wang, Lei Li, Wei Bai, Zhongtao Ding, *Corrosion Science*, 53 (2011) 1186-1193.